Evaluation of the Catalytic Mechanism of AICAR Transformylase by pH-Dependent Kinetics, Mutagenesis, and Quantum Chemical Calculations

Jae Hoon Shim,[†] Mark Wall,[†] Stephen J. Benkovic,*[,†] Natalia Díaz,[‡] Dimas Suárez,[§] and Kenneth M. Merz, Jr.[§]

Contribution from 414 Wartik Laboratory, Department of Chemistry, The Pennsylvania State University, University Park, Pennsylvania 16802, Departamento de Química Física y Analítica, Universidad de Oviedo, Julián Clavería 33006, Oviedo, Spain, and 152 Davey Laboratory, Department of Chemistry, The Pennsylvania State University, University Park, Pennsylvania 16802-6300

Received January 2, 2001

Abstract: The catalytic mechanism of 5-aminoimidazole-4-carboxamide ribonucleotide transformylase (AICAR Tfase) is evaluated with pH dependent kinetics, site-directed mutagenesis, and quantum chemical calculations. The chemistry step, represented by the burst rates, was not pH-dependent, which is consistent with our proposed mechanism that the 4-carboxamide of AICAR assists proton shuttling. Quantum chemical calculations on a model system of 5-amino-4-carboxamide imidazole (AICA) and formamide using the B3LYP/6-31G* level of theory confirmed that the 4-carboxamide participated in the proton-shuttling mechanism. The result also indicated that the amide-assisted mechanism is concerted such that the proton transfers from the 5-amino group to the formamide are simultaneous with nucleophilic attack by the 5-amino group. Because the process does not lead to a kinetically stable intermediate, the intramolecular proton transfer from the 5-amino group through the 4-carboxamide to the formamide proceeds in the same transition state. Interestingly, the calculations predicted that protonation of the N3 of the imidazole of AICA would reduce the energy barrier significantly. However, the pK_a of the imidazole of AICAR was determined to be 3.23 ± 0.01 by NMR titration, and AICAR is likely to bind to the enzyme with its imidazole in the free base form. An alternative pathway was suggested by modeling Lys266 to have a hydrogen-bonding interaction with the N3 of the imidazole of AICAR. Lys266 has been implicated in catalysis based on mutagenesis studies and the recent X-ray structure of AICAR Tfase. The quantum chemical calculations on a model system that contains AICA complexed with $CH_3NH_3^+$ as a mimic of the Lys residue confirmed that such an interaction lowered the activation energy of the reaction and likewise implicated the 4-carboxamide. To experimentally verify this hypothesis, we prepared the K266R mutant and found that its k_{cat} is reduced by 150-fold from that of the wild type without changes in substrate and cofactor K_m values. The k_{cat}-pH profile indicated virtually no pH-dependence in the pH range 6−10.5. The results suggest that the ammonium moiety of Lys or Arg is important in catalysis, most likely acting as a general acid catalyst with a pK_a value greater than 10.5. The H267A mutant was also prepared since His267 has been found in the active site and implicated in catalysis. The mutant enzyme showed no detectable activity while retaining its binding affinity for substrate, indicating that it plays a critical role in catalysis. We propose that His267 interacts with Lys266 to aid in the precise positioning of the general acid catalyst to the N3 of the imidazole of AICAR.

Introduction

Aminoimidazole-4-carboxamide ribonucleotide transformylase (AICAR Tfase[1]) catalyzes the penultimate reaction in the de novo purine biosynthetic pathway, producing formyl-AICAR (FAICAR) from AICAR using 10-formyltetrahydrofolate (10-f-H_4F) as the formyl donor. It exists as one domain of a bifunctional enzyme that also contains IMP Cyclohydrolase (IMP CHase) that catalyzes the final reaction of the pathway (Scheme 1). Because of the large demand for purines by cancer cells, AICAR Tfase has been targeted by antifolate inhibitors in chemotherapy along with glycinamide ribonucleotide transformylase (GAR Tfase), another folate-dependent transformylase in the pathway. GAR Tfase catalyzes a formyl transfer using the same cofactor, 10-f-H_4F, and has been extensively studied in terms of kinetics and structure. A detailed catalytic mechanism involving active-site residues has been established from

* To whom correspondence should be addressed. Telephone: 814-865-2882. Fax: 814-865-2973.

[†] 414 Wartik Laboratory, Department of Chemistry, The Pennsylvania State University.

[‡] Universidad de Oviedo.

[§] 152 Davey Laboratory, Department of Chemistry, The Pennsylvania State University.

(1) Abbreviations used: AICAR, 5-aminoimidazole-4-carboxamide ribonucleotide; AICAR Tfase, AICAR transformylase; IMP CHase, IMP cyclohydrolase; 10-f-H_4F, (6*R*,α*S*)-10-formyl-5,6,7,8-tetrahydrofolic acid; 10-f-H_2F, 10-formyl-7,8-dihydrofolic acid, FAICAR, 5-formyl-AICAR.; GAR Tfase; glycinamide ribonucleotide transformylase; AICA, 5-amino-4-carboxamide imidazole; IRC, intrinsic reaction coordinate; PES, potential energy surface; UAHF, united atom Hartree−Fock; PCM, polarizable continuum model; NPA, natural population analysis; ZPVE, zero-point vibrational energy; TS, transition state; PA, proton affinity; thio-AICAR, 5-amino-1-β-D-ribofuranosylimidazole-4-thiocarboxamide 5′-phosphate; thio-AICA, 5-amino-4-thiocarboxamide imidazole; B3LYP, Becke3, Lee, Yang, Parr.

10.1021/ja010014k CCC: $20.00
Published on Web 04/25/2001

Scheme 1. AICAR Tfase-IMP CHase reaction

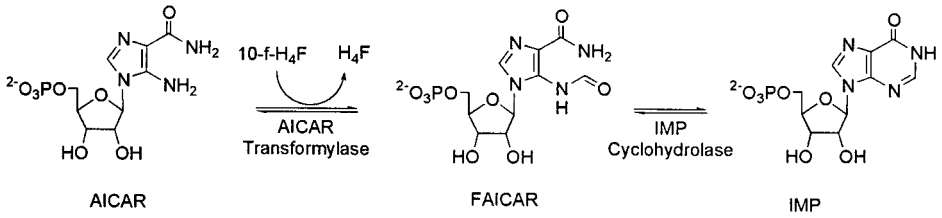

X-ray crystallographic structures and kinetic analysis of the wild-type enzyme and selected mutants.[2]

Because both transformylases catalyze a similar chemical reaction, that is a transfer of a formyl group from the same cofactor, they were anticipated to have similar catalytic mechanisms. However, several lines of evidence implied that two enzymes might operate differently. First of all, the amino acid sequence homology between the two transformylases is quite low. Although a similar grouping of amino acids (His, Asp, and Asn) that acts as a catalytic triad in GAR Tfase was also found in AICAR Tfase, these amino acids are not catalytic residues as revealed by mutation analysis.[3] Second, the transformylation of AICAR by 10-formyldihydrofolate (10-f-H_2F; kinetically equivalent to 10-f-H_4F) is an unfavorable reaction with a K_{eq} of 0.024.[4] AICAR Tfase is found as a domain of the bifunctional enzyme throughout all species characterized to date from *Escherichia coli* to human, an arrangement that couples the unfavorable formation of FAICAR with the highly favorable cyclization reaction catalyzed by IMP CHase. Third, our previous studies on substrate analogues revealed that the amide moiety in AICAR is essential for formyl transfer, and its conformation is important in the binding to the enzyme active site. We proposed that the amide assists in the required proton shuttling from the 5-amino group to the N-10 of the folate in the tetrahedral transition state.[4] Fourth, a recent partially refined crystallographic structure of the bifunctional enzyme has indicated that Lys266 and His267[5] are two potentially important catalytic residues in the active site.[6] Site-directed mutation of these residues to Ala were found to abolish the transformylase activity of the mutants, although they still retain binding affinity for AICAR.[7]

In this report, we have extended our investigation on the catalytic mechanism of AICAR Tfase by analyzing the roles of key active-site residues through mutagenesis and the kinetic analysis of the mutants. Quantum mechanical calculations were also carried out on model systems for formyl transfer to provide further insights into the role of the 4-carboxamide of AICAR in catalysis.

Materials and Methods

Materials. AICAR were purchased from Sigma and 10-f-H_2F was prepared as described previously.[4] Ni-NTA agarose was purchased from QIAGEN. Pfu polymerase was purchased from Strategene, and DpnI from New England Biolab. D_2O, NaOD, DCl, and 3-(trimethylsilyl)-propionic-2,2,3,3-d_4 acid were purchased from Aldrich. All common buffers and reagents were obtained from VWR, Fisher, Sigma, or Aldrich.

Site-Directed Mutagenesis. Site-directed mutagenesis was performed using the QuickChange (Strategene) method. The primers used were: for the H267A mutant, 5-GCCTCTTTCAAAGCTGTCAACCCAGC-3′ and 5′-GCTGGGCTGACAGCTTTGAAAGAGGC-3′; for the K266R mutant, 5′-GCCCTGCCTTCTTTCAGACATGTCAGCCCAGC-3′ and 5′-GCTGGGCTGACATGTCTGAAAGAGGCAGCGGC-3′ (mutated sites are underlined). PCR reactions consisted of 50 ng of the pET28a plasmid containing purH cDNA, 0.2 mM each dNTP, 0.25 μM each primer, 1X Pfu buffer, and 2.5 units of Pfu DNA polymerase in a total volume of 100 μL. PCR was carried out in one cycle of 30 s at 95 °C and then in 16 cycles using 30 s at 95 °C followed by 1 min of 65 °C and 14 min of 68 °C. After PCR amplification, the reaction mixture was treated with 20 units of DpnI for 1 h to digest the parental plasmid. About 3−4 μL of the DpnI-treated PCR mixture was directly transformed into DH5α cells by electroporation or by using $CaCl_2$ transformation. Transformed cells were selected on LB plates containing 25 μg/mL kanamycin. Plasmid DNA was purified from transformants using Qiagen prep columns. The mutant enzymes, H267A and K266R or the wild-type enzyme were prepared as described previously.[4]

pK_a Determination of the Imidazole of AICAR. An AICAR solution (~5 mM) was prepared in D_2O that contains 2 mM of 3-(trimethylsilyl)-propionic-2,2,3,3-d_4 acid and 100 mM NaCl. Solutions whose pH ranged from 1.5 to 8 were prepared by adding DCl or NaOD and by measuring the pH with a Radiometer America pH electrode. No correction was made for the deuterium isotope effect as the pK_a shift in D_2O solution is largely offset by the isotope effect at the glass electrode (−0.4 unit).[8] ^{1}H NMR spectra were obtained for each AICAR solution at a different pH to measure chemical shift values of the C-2 proton. The chemical shift data were fitted to eq 1 to calculate the pK_a value of the imidazole ring of AICAR.[8]

$$\delta_{obs} = \delta_{H+} + (\delta_{H0} - \delta_{H+}) \times 10^{-pKa}/(10^{-pH} + 10^{-pKa}) \quad (1)$$

In this eq, δ_{obs} is the observed chemical shift of the C-2 proton, δ_{H+} is the chemical shift of the C-2 proton of the fully protonated imidazole, and δ_{H0} is the chemical shift of the C-2 proton of the unprotonated imidazole.

Kinetic Measurements. All kinetic measurements were performed at 25 °C in a buffer that contained 50 mM cacodylic acid, 25 mM ethanolamine, 25 mM Tris, and 25 mM potassium chloride (CTEK). The ionic strength of this buffer remains constant over the pH range, 6−10.5. Enzyme assays were carried out in a 1 mL cuvette thermostated on a Cary spectrophotometer. AICAR Tfase was assayed using AICAR and 10-f-H_2F by following the production of H_2F at 298 nm ($\Delta\epsilon$ = 18.0 mM^{-1} cm^{-1}). The value of $\Delta\epsilon$ remained unchanged over the pH range used. IMP CHase was assayed by following IMP production at 248 nm ($\Delta\epsilon$ = 5.7 mM^{-1} cm^{-1}).

Stopped-flow experiments were performed on an Applied Photophysics Kinetic Spectrometer (Cambridge, England) that has a thermostated sample cell. Absorbance measurements were conducted at 298 nm with a 0.5 mm slit width. In pre-steady-state burst kinetics, enzyme (2.5 μM) was preincubated with a saturating amount of 10-f-H_2F, and reacted with a saturating amount of AICAR. In most

(2) Shim, J. H.; Benkovic, S. J. *Biochemistry* **1999**, *38*, 10024−10031.
(3) Rayl, E. A.; Moroson, B. A.; Beardsley, G. P. *J. Biol Chem.* **1996**, *271*, 2225−2233.
(4) Wall, M.; Shim, J. H.; Benkovic, S. J. *Biochemistry* **2000**, *39*, 11303−11311.
(5) Numbering of the amino acid of our sequence is greater by 1 than the Beardsley's sequence[3] because of the difference in the N-terminal sequence (Sugita, T.; Aya, H.; Ueno, M.; Ishizuka, T.; Kawashima, K. *J. Biochem. (Tokyo)* **1997**, *122*, 309−313).
(6) Wilson, I. A. Personal Communication.
(7) Beardsley, G. P.; Rayl, E. A.; Gunn, K.; Moroson, B. A.; Seow, H.; Anderson, K. S.; Vergis, J.; Fleming, K.; Worland, S.; Condon, B.; Davies, J. In *Purine and Pyrimidine Metabolism in Man*; Griesmacher, A., Ed.; Plenum Press: New York, 1997; pp 221−226.
(8) Markley, J. L. *Acc. Chem. Res.* **1975**, *8*, 70−80.

Scheme 2. Model System for Formyl Transfer and Various AICA Species Used in Calculations

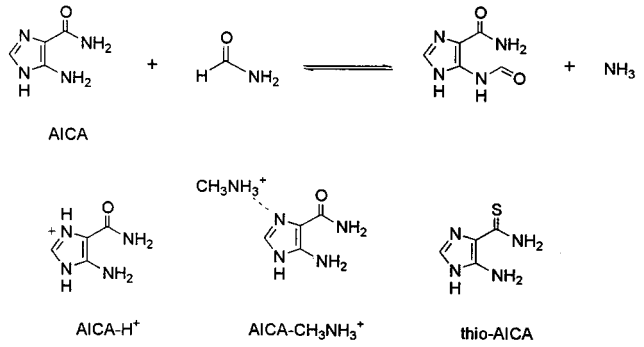

experiment, 5−8 traces were recorded and averaged for data analysis. Data were collected over a given time interval by an Acorn computer. All data were analyzed by a nonlinear least-squares computer program provided by Applied Photophysics or transferred to a PC to be fitted to the appropriate equations using nonlinear least-squares fitting program in KaleidaGraph (v. 3.0). Data from saturation kinetics were fitted to the Michaelis−Menten equation to obtain k_{cat} and K_m values.

Fluorescence Titrations. The thermodynamic dissociation constants (K_d) for AICAR from the enzyme were measured by fluorescence titration on a FluoroMax-2 (Jobin Yvon-SPEX) spectrofluorometer. The binding of AICAR to the enzyme was followed by measuring the quenching of the intrinsic enzyme fluorescence at 340 nm upon excitation at 290 nm as a function of AICAR concentration. In this experiment, a solution of tryptophan with a fluorescence similar to that of the enzyme solution was titrated to correct for the absorbance caused by added AICAR. The data were fit to a hyperbolic equation.

Quantum Chemical Calculations. Molecular geometry optimizations followed by analytical frequency calculations were performed at the B3LYP/6-31G* level of theory[9] using the Gaussian 98 suite of programs.[10] B3LYP/6-31G* intrinsic reaction coordinate (IRC) calculations[11] were carried out to confirm the reaction paths on the potential energy Surface (PES). The performance of the B3LYP method to study the aminolysis reaction of amides has been tested in previous work on the aminolysis of 2-azetidinone[12] with the B3LYP energies and structures comparing favorably with those obtained using the sophisticated composite level of theory, G2(MP2,SVP).[13] Atomic charges were computed by carrying out a natural population analysis (NPA) using the corresponding B3LYP/6-31G* density matrices.[14]

First, we characterized the structure and energetics of the model compounds, 5-amino-4-carboxamide-imidazole (AICA) and its N3-protonated form (AICA-H^+) (Scheme 2). We also considered a third model system (AICA-$CH_3NH_3^+$) in which the AICA imidazole ring and its 4-carboxamide group are bound to a methylammonium cation through two N−H···N hydrogen bonds simulating thus possible contacts of the AICAR substrate with the essential Lys residue in the AICAR Tfase active site. For these model systems, we analyzed the intramolecular 5-amino → 4-carboxamide proton-transfer process for the proposed catalytic role of the 4-carboxamide group. Subsequently, the aminolysis reaction of the three models with formamide was studied as a model system for the AICAR Tfase mechanism of reaction. Two different mechanisms were examined theoretically: an uncatalyzed pathway and an aminolysis process assisted by the carboxamide functionality. The effect of thiocarboxamide on the aminolysis process was also examined using the unprotonated form of 5-amino-4-thiocarboxamide imidazole (thio-AICA) and its $CH_3NH_3^+$-interacting form.

The relative pK_a trend in aqueous solution for a series of AICA analogues with various substitutions at C-4 was computed by combining solvation energies and the B3LYP/6-31G* gas-phase energies involved in the following process:

$$B + H_3O^+ \overset{\Delta G_a}{\rightleftharpoons} B\text{-}H_3O^+ \qquad (2)$$

We used the united atom Hartree−Fock (UAHF) parametrization[15] of the polarizable continuum model (PCM)[16] including both electrostatic and nonelectrostatic solute−solvent interactions and simulating water as solvent. The solvation Gibbs energies $\Delta G_{solvation}$ were then computed from single-point B3LYP/6-31G* PCM-UAHF calculations on the B3LYP/6-31G* gas-phase geometries. When PCM calculations are used to calculate standard state Gibbs energies of conjugate acids and bases in solution, the acid dissociation constant pK_a can be obtained using the following equation:

$$pK_a = \frac{-\Delta G_a}{2.303RT} \qquad (3)$$

where

$$\Delta G_a = \Delta G_{gas-phase} + \Delta G_{solvation}(B{-}H_3O^+) - \Delta G_{solvation}(B) - \Delta G_{solvation}(H_3O^+) \qquad (4)$$

Thus, the calculation of the pK_a values should be straightforward from eqs 3 and 4. Unfortunately, the agreement of such calculations with the experimental values is notoriously difficult, because very high levels of theory are required to accurately predict the proton affinities and solvation energies of ions. In practice, only the estimation of *relative* pK_a's of related compounds may be done with confidence using dielectric continuum models.

Results

pH Dependence of k_{burst}. The AICAR Tfase reactions in the pH range 6−10.5 showed pre-steady-state bursts of product formation. These rates were about 7−10 times higher than the steady-state rates, and the amplitudes are very close to the total concentration of the enzyme used. We have assigned these rates (k_{burst}) to the chemical step, in the absence of data implicating a slower step preceding the chemical step. The k_{burst} values in this pH range showed no dependence on pH (Figure 1) so that no ionizable functional group or residue involved in catalysis was detected.

Preparations of Mutant Enzymes. The mutant H267A and K266R plasmids were constructed by the QuickChange procedure. Sequencing of the entire structural gene of the mutant proteins confirmed that only the desired mutation was introduced. They were purified to homogeneity by the same

(9) (a) Hehre, W. J.; Radom, L.; Pople, J. A.; Schleyer, P. v. R. *Ab Initio Molecular Orbital Theory*; John Wiley & Sons Inc.: New York, 1986. (b) Becke, A. D. Exchange-Correlation Approximation in Density-Functional Theory. In *Modern Electronic Structure Theory Part II*; Yarkony, D. R., Ed.; World Scientific: Singapore, 1995.

(10) Frisch, M. J.; Trucks, G. W.; Schlegel, H. B.; Scuseria, G. E.; Robb, M. A.; Cheeseman, J. R.; Zakrzewski, V. G.; Montgomery, J. A., Jr.; Stratmann, R. E.; Burant, J. C.; Dapprich, S.; Millam, J. M.; Daniels, A. D.; Kudin, K. N.; Strain, M. C.; Farkas, O.; Tomasi, J.; Barone, V.; Cossi, M.; Cammi, R.; Mennucci, B.; Pomelli, C.; Adamo, C.; Clifford, S.; Ochterski, J.; Petersson, G. A.; Ayala, P. Y.; Cui, Q.; Morokuma, K.; Malick, D. K.; Rabuck, A. D.; Raghavachari, K.; Foresman, J. B.; Cioslowski, J.; Ortiz, J. V.; Stefanov, B. B.; Liu, G.; Liashenko, A.; Piskorz, P.; Komaromi, I.; Gomperts, R.; Martin, R. L.; Fox, D. J.; Keith, T.; Al-Laham, M. A.; Peng, C. Y.; Nanayakkara, A.; Gonzalez, C.; Challacombe, M.; Gill, P. M. W.; Johnson, B.; Chen, W.; Wong, M. W.; Andres, J. L.; Gonzalez, C.; Head-Gordon, M.; Replogle, E. S.; Pople, J. A. *Gaussian 98*, revision A.6; Gaussian, Inc.: Pittsburgh, PA, 1998.

(11) (a) Fukui, K. *Acc. Chem. Res.* **1981**, *14*, 363−368. (b) González, C.; Schlegel, H. B. *J. Phys. Chem.* **1990**, *94*, 5523−5529.

(12) (a) Díaz, N.; Suárez, D.; Sordo. T. L. *Chem. Eur. J.* **1999**, *5*, 1045−1054. (b) Díaz, N.; Suárez, D.; Sordo. T. L *J. Am. Chem. Soc.* **2000**, *122*, 6710−6719.

(13) Curtiss, L. A.; Redfem, P. C.; Smith, B. J.; Radom, L. *J. Chem. Phys.* **1996**, *104*, 5148−5152.

(14) Reed, A. E.; Weinstock, R. B.; Weinhold, F. *J. Chem. Phys.* **1985**, *83*, 735−746.

(15) Barone, V.; Cossi, M.; Tomasi, J. *J. Chem. Phys.* **1997**, *107*, 3210−3221.

(16) Tomasi, J.; Persico, M. *Chem. Rev.* **1994**, *94*, 2027−2094.

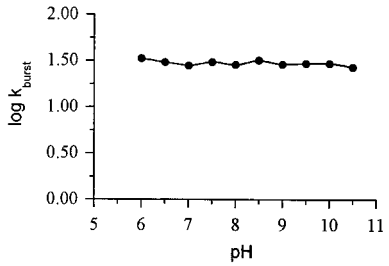

Figure 1. pH dependence of k_{burst} for the wild type.

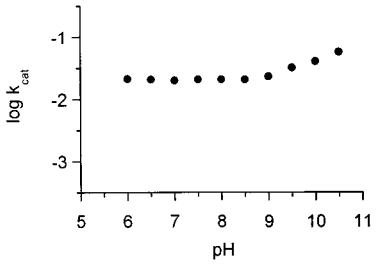

Figure 2. pH dependence of k_{cat} for the K266A mutant.

Table 1. Summary of Kinetic Parameters for AICAR Tfase at pH 7.5 in CTEK Buffer

	k_{cat} (s^{-1})	K_m (AICAR) (μM)	K_m (10-f−H_2F) (μM)
wild type	3.3 ± 0.1	1.9 ± 0.4	7.6 ± 0.6
K266R	0.021 ± 0.001	0.5 ± 0.1	4.3 ± 0.4
H267A	NA[a]	NA	NA

[a] NA = no activity.

procedure as for the wild-type enzyme, and their level of expression was very similar to that of the wild type.

Characterization of the Mutant Enzymes. Consistent with the report by Beardsley,[3] the H267A enzyme showed no detectable AICAR Tfase activity while retaining full IMP CHase activity. Furthermore, it binds AICAR with a K_d value of 13.2 $\pm$ 2.2 μM determined by a fluorescence titration. The same experiment yielded a K_d value of 5.2 $\pm$ 1.2 μM for the wild type.

However, the K266R enzyme gave detectable AICAR Tfase activity in its cell lysate. Its k_{cat} value is 0.021 $\pm$ 0.001 s^{-1}, 150-fold lower than that of the wild type, although the K_m values for the substrates were very similar to those of the native enzyme (Table 1). Unlike the wild type, the K266R enzyme showed no pre-steady-state burst in the pH range used, consistent with the k_{cat} values measuring a rate-limiting chemistry step. The k_{cat} values, like k_{burst} for the native enzyme, showed no pH dependence at low pH (6 to 9) but increased slowly at higher pH after pH 9 (Figure 2). However, the limiting slope of the profile at high pH is less than 0.5.

pK_a of the Imidazole of AICAR. Since the quantum chemical calculations suggested that protonation of the imidazole of AICAR is important in lowering the activation energy of the transformylation (vide infra), we measured the pK_a value of the imidazole in solution, through monitoring the change in the chemical shift of the C-2 proton at various pHs. AICAR acted as a buffer in maintaining pH and the addition of NaCl (100 mM) minimized changes in ionic strength. The chemical shift of the C-2 proton underwent changes from 8.65 to 7.52 ppm as the pH increased from 1.5 to over 6 (Figure 3). The pK_a value was calculated by fitting the curve to eq 1 to give 3.23 $\pm$ 0.01.

Theoretical Analysis of the AICA Model System. The calculated equilibrium geometry of the AICA isomer [**AICA-(1)** in Figure 4A] shows a pyramidal 5-amino group generated through an intramolecular N−H···O contact of the amino group hydrogen with the oxygen of the carboxamide at a typical hydrogen bond distance of 2.129 Å. This conformation coincides with that observed in the AICAR X-ray structure[17] which is assumed to be unchanged upon binding of AICAR to the enzyme.

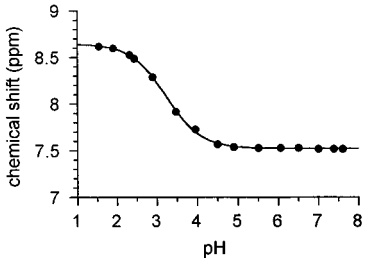

Figure 3. ^{1}H NMR titration curves for the imidazole C-2 proton of AICAR.

The structure **AICA(1)** can undergo an intramolecular proton transfer to the amide O atom through the transition state (TS) structure **TS_H** to give the isomer **AICA(2)** which is 16.7 kcal/mol less stable than the ground-state isomer **AICA(1)** (Figure 4A). The **TS_H** structure is very close both in geometry and energy to **AICA(2)** which is only 0.5 kcal/mol more stable than **TS_H** on the electronic B3LYP/6-31G* PES. After taking into account zero-point vibrational energy (ZPVE) corrections, **AICA(2)** is 1.6 kcal/mol less stable than **TS_H**, that is the relative stabilities of **TS_H** and **AICA(2)** are reversed. From these results, the existence of prereactive complexes or reaction intermediates having the carboxamide group in its protonated form would be only transient although the intramolecular hydrogen bond between the 5-amino and 4-carboxamide groups in **AICA(1)** might be kinetically relevant to promote the elongation of the N−H bond during the aminolysis reaction.

The uncatalyzed mechanism for the aminolysis reaction between AICA and formamide has been chosen to model the enzyme-catalyzed process. It proceeds through the concerted 1,2-addition of one H−NH bond to the formamide C−N bond and features the simultaneous rupture of this amide bond and the transfer of the H atom to the leaving ammonia molecule. The TS describing this process corresponds to the structure **TS_C** whose transition vector consists basically of the motion of the H atom between the two N reactive atoms (Figure 4B). The geometry of **TS_C** characterizes this TS as a tight structure, that is the H being transferred is located in an intermediate position between the reactive N atoms with N−H distances of 1.357 and 1.253 Å; the new C−N bond is quite advanced (1.786 Å); the formamide C−N bond is barely cleaved (1.592 Å). This concerted mechanism presents a high-energy barrier of 40.3 kcal/mol on the electronic B3lYP/6-31G* PES.

Introducing participation by the carboxamide in the transfer process requires the carboxamide group to be protonated along the reaction coordinate to facilitate the proton transfer to the leaving N atom. A TS for the amide-assisted aminolysis of formamide reacting with AICA (**TS_C-amide** in Figure 4C) was located on the electronic B3LYP/6-31G* PES. At **TS_C-amide**, the deprotonated 5-amino group of AICA is attacking the carbonyl C atom of formamide while the H atom originally attached to the amino group is being transferred from the amide O atom of AICA to the leaving ammonia molecule. According to the bond distances of the reactive bonds, **TS_C-amide** has more

(17) Adamiak, D. A.; Saenger, W. *Acta Crystallogr., Sect. B* **1979**, *35*, 924−938.

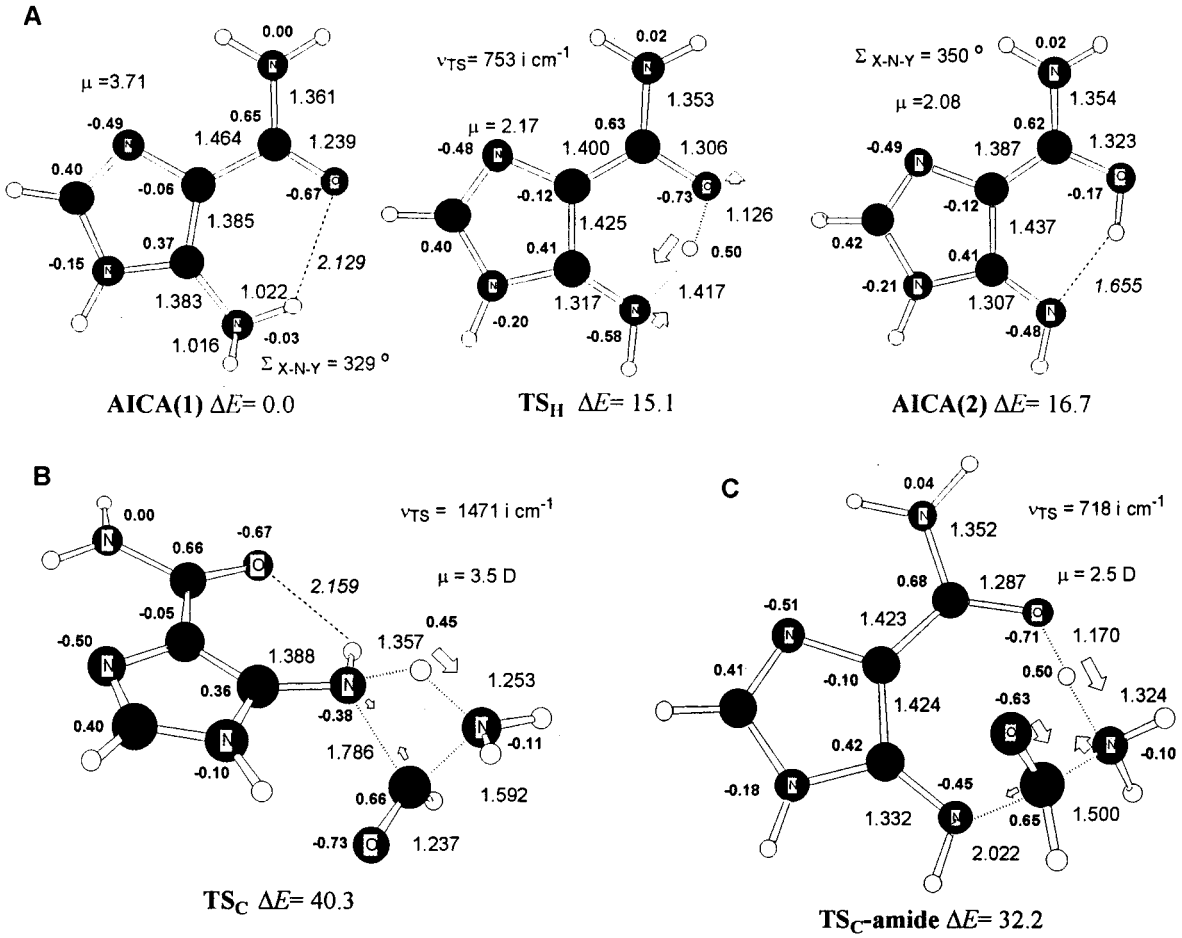

Figure 4. AICA model system. (A) Optimized structures of the critical structures involved in the 5-amino → 4-carboxamide proton transfer for the AICA model studied. Distances in Å. Natural population analysis (NPA) charges with hydrogens summed into heavy atoms in boldface characters. B3LYP/6-31G* relative energies including the ZPVE correction (Δ*E* in kcal/mol) are also shown. (B) Optimized structure of the TS for the uncatalyzed aminolysis reaction between formamide and the AICA model. (C) Optimized structure of the TS for the amide-assisted aminolysis reaction between formamide and the AICA model. Distances in Å. NPA charges with hydrogens summed into heavy atoms in boldface characters. B3LYP/6-31G* relative energies including the ZPVE correction (Δ*E* in kcal/mol) are also shown.

reactant-like character than **TS$_C$** (i.e., the bond-forming and -breaking C−N distances are 2.022 and 1.500 Å, respectively) although the H atom being transferred is simultaneously bound to the donating O atom (1.170 Å) and the accepting N atom (1.324 Å). The energy barrier of **TS$_C$-amide** (32.2 kcal/mol) predicts the catalytic effect of the 4-carboxamide group is 8.1 kcal/mol.

To determine whether stable intermediates form in the amide-assisted process, we performed IRC calculations followed by energy minimizations on the electronic B3LYP/6-31G* PES. These calculations revealed that the proton transfer from the 5-amino group toward the formamide N atom takes place with the assistance of the O atom of the AICA 4-carboxamide group all along the reactant channel on the PES, so that the initial stages of the process resemble a 5-amino → 4-carboxamide proton-transfer event. Nevertheless, we found that **TS$_C$-amide** is directly connected on the ZPVE-corrected energy profile with an **AICA(1)** complexed with formamide that interacts through a single hydrogen bond with the 5-amino moiety of the **AICA-(1)** isomer. Hence, the reaction mechanism through **TS$_C$-amide** follows a concerted pathway in which the initial 5-amino → 4-carboxamide proton transfer is followed by a proton transfer to the formamide with simultaneous nucleophilic attack. In this mechanism, the 4-carboxamide group linked to the H-atom being transferred plays a passive role stabilizing the configurations along the reaction pathway.

Table 2. B3LYP/6-31G* Proton Affinities (kcal/mol) of Various 4-Substitued 5-Amino-imidazole Compounds

Structure	PA	δpK_a(N3)[a]	Structure	PA	δpK_a(N3)
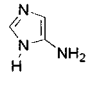	235.4	0.0	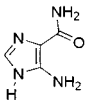	225.8	-5.8
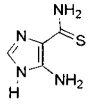	222.0	-8.0	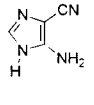	221.4	-4.3
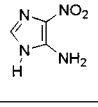	219.2	-5.4			

[a] pK_a difference with respect to the unsubstitued.

Theoretical Analysis of the AICA-H$^+$ and the AICA-CH$_3$NH$_3^+$ Model Systems. Because of the possibility that protonation of AICAR might occur in the enzyme-catalyzed process, we extended our analysis to such species. The calculated proton affinity (PA) in the gas-phase for protonation on the N3 atom of **AICA(1)** to yield the structure **AICA(1)-H$^+$** is 225.8 kcal/mol (Table 2 and Figure 5A). This PA is 9.6 kcal/mol lower than that of an unsubsituted AICA species, owing to electron withdrawal by the 4-carboxamide group. Comparing the ge-

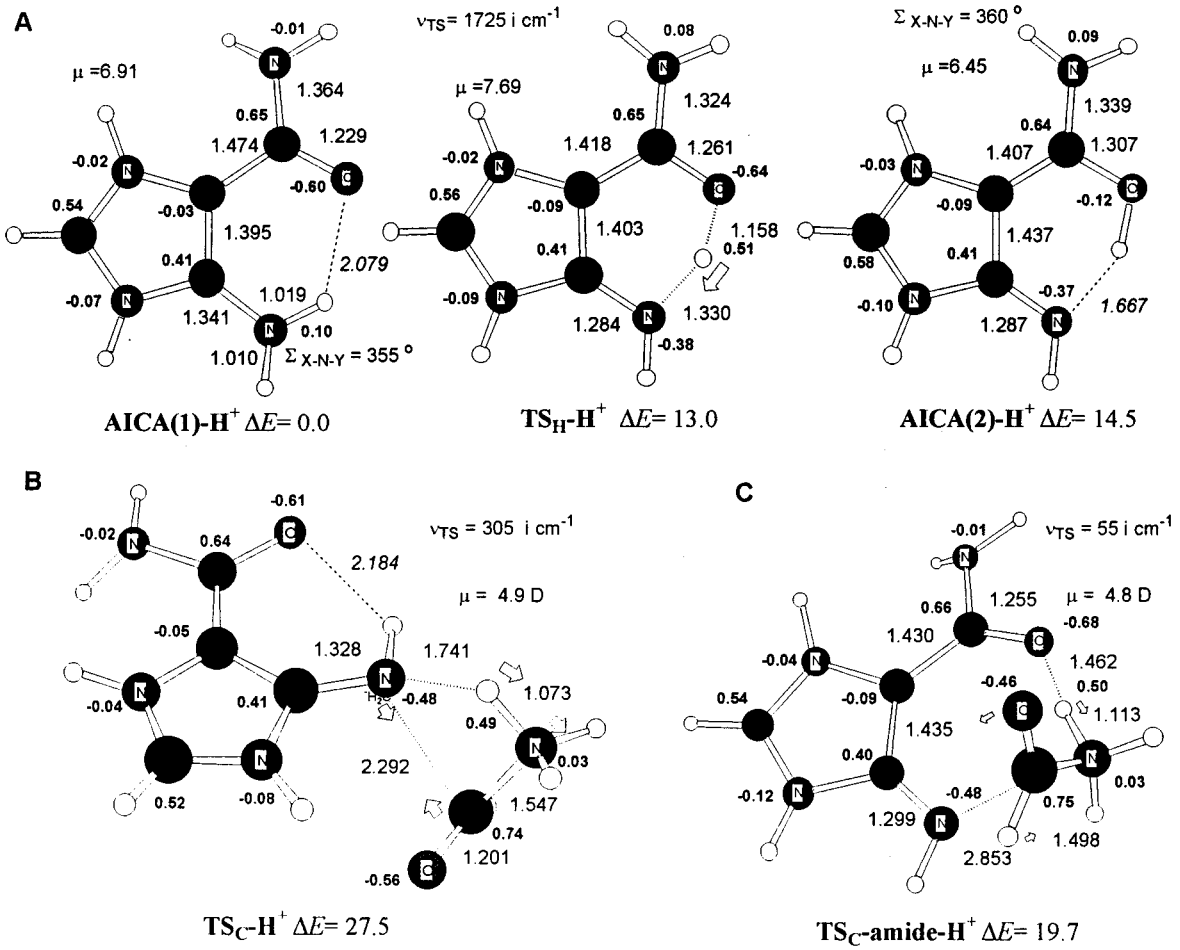

Figure 5. AICA-H^+ model system. (A), (B), and (C) The same structural descriptions as in Figure 4.

ometry and charge distribution of the **AICA(1)** and **AICA(1)-H^+** structures, it is clear that the lone pair of the 5-amino group is conjugated with the imidazole ring as a consequence of protonation (e.g., the C5−N bond is shortened by 0.04 Å, the 5-amino group, which donates 0.13 e upon protonation, is nearly coplanar with the imidazole ring).

The X-ray crystallographic structure which features a bound AICAR reveals the proximity of a Lys side chain to the imidazole moiety of AICAR. The interaction between **AICA-(1)** and methylammonium, a surrogate for the Lys, gives the complex **AICA(1)···$CH_3NH_3^+$** in Figure 6A with a binding energy of −31.9 kcal/mol. In this complex, the lone pair of the N3 atom establishes a short hydrogen bond of 1.798 Å with the ammonium group. The second NH···N contact (1.962 Å) links the $CH_3NH_3^+$ moiety with the lone pair of the carboxamide N atom. Through these relatively strong hydrogen-bonding interactions, the $CH_3NH_3^+$ moiety accepts 0.13 e according to NPA charges. We also note that the sum of the bond angles around the carboxamide N atom (331°) indicates that the amide resonance must be substantially reduced by the presence of the $CH_3NH_3^+$ cation (Figure 6A).

We now trace the energetics of the proton transfer from the 5-amino group to the oxygen of the carboxamide. Both the amino and carboxamide groups are conjugated with the imidazole ring. Thus, the reinforced electron-withdrawing ability of the protonated imidazole would stabilize the basic form of both groups and, therefore, the influence of N3-protonation on the 5-amino → 4-carboxamide proton-transfer pathway would be moderate due to the partial cancellation of substituent effects. Our calculations predict that the **AICA(2)-H^+** isomer, related to **AICA(1)-H^+** via intramolecular proton transfer, is 14.5 kcal/mol above **AICA(1)-H^+** (Figure 5A). This figure is only 2.2 kcal/mol lower than the energy difference between the neutral **AICA(1)** and **AICA(2)** structures. In the case of the $CH_3NH_3^+$-interacting models, the N−H···N contact with the carboxamide group precludes the n → p*conjugation of the lone pair of the carboxamide N atom throughout the imidazole ring when the amide O atom becomes protonated (Figure 6A). This effect results in the **AICA(2)···$CH_3NH_3^+$** structure being destabilized by ∼2 kcal/mol with respect to its isolated counterpart. Most importantly, the TSs for proton transfer, **TS_H-H^+** and **TS_H···$CH_3NH_3^+$**, are 1.5 kcal/mol more stable than **AICA(2)-H^+** and **AICA(2)···$CH_3NH_3^+$**, respectively (Figures 5A and 6A). Therefore, as in the case of the unprotonated AICA model, the 5-amino → 4-carboxamide proton transfer does not lead to stable structures in either the N3-protonated or the $CH_3NH_3^+$-interacting forms of AICA; the reversion of **AICA(2)-H^+** and **AICA-(2)···$CH_3NH_3^+$** into their respective ground-state isomer thus remains a barrierless process.

As before, we now compute the effect of N3 protonation on our model reaction for the transfer process. The increased acidity of the 5-amino group upon protonation of the N3 atom or binding with $CH_3NH_3^+$ is now reflected in the geometry of the corresponding **TS_C-H^+** and **TS_C···$CH_3NH_3^+$** transition states (Figures 5B and 6B) for the uncatalyzed (no amide participation) reaction. In contrast with the intramolecular 5-amino → 4-carboxamide proton transfer, the intermolecular proton transfer to the formamide moiety is practically completed in these TSs as reflected in the bond distances of the breaking and forming N−H bonds which are 1.741 and 1.073 Å at **TS_C-H^+** (1.654 and 1.094

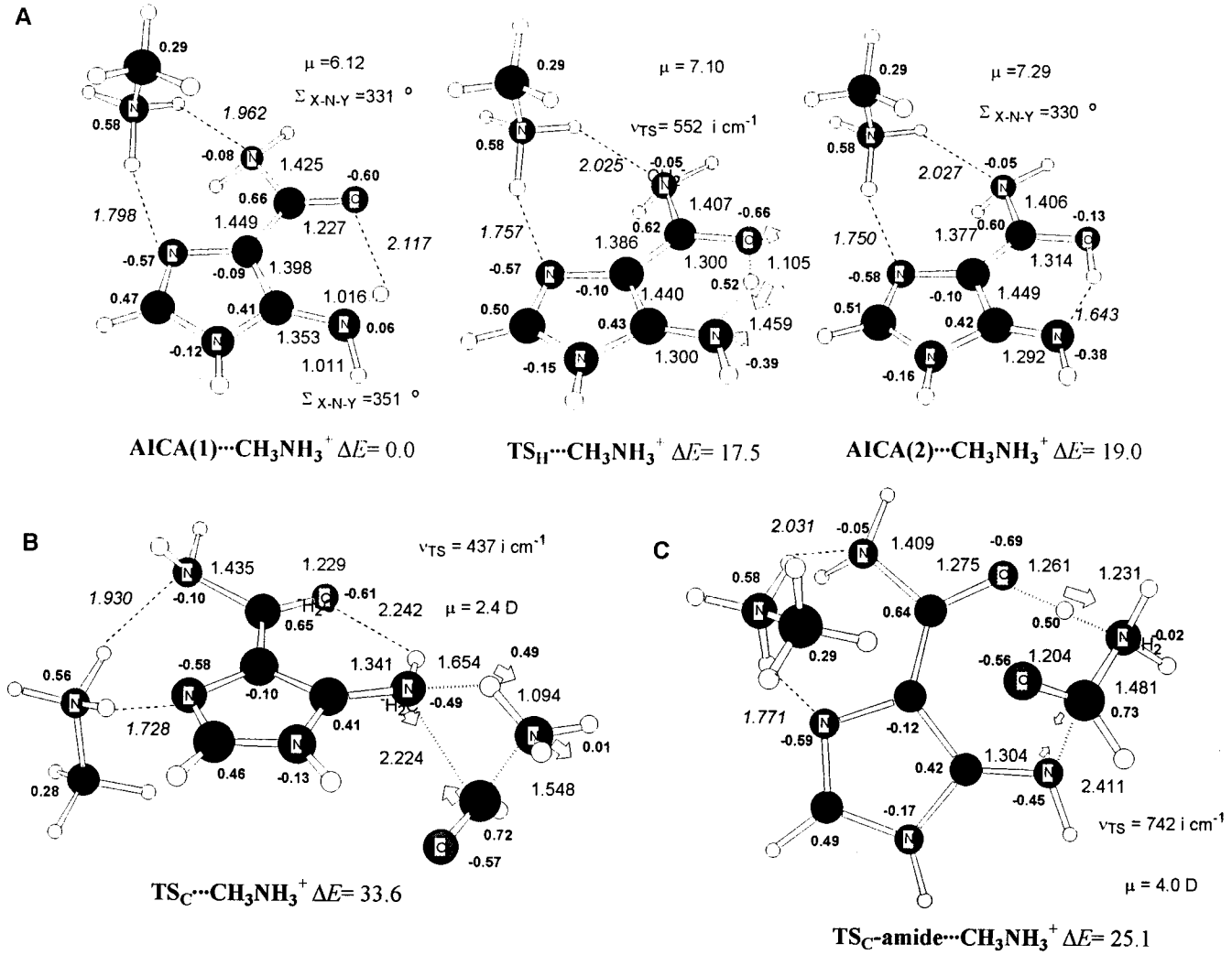

Figure 6. AICA-$CH_3NH_3^+$ model system. (A), (B), and (C) The same structural descriptions as in Figure 4.

Å at $\mathbf{TS_C\cdots CH_3NH_3^+}$). Reciprocally, the nucleophilicity of the 5-amino group is substantially reduced and that leads to a transition state in which the developing C−N bond is elongated from 1.786 Å at $\mathbf{TS_C}$ to 2.292 and 2.224 Å at $\mathbf{TS_C\text{-}H^+}$ and $\mathbf{TS_C\cdots CH_3NH_3^+}$. The calculated energy barriers for $\mathbf{TS_C\text{-}H^+}$ and $\mathbf{TS_C\cdots CH_3NH_3}$+ are 27.5 and 33.6 kcal/mol, relative to the ground states, $\mathbf{AICA(1)\text{-}H^+}$ and $\mathbf{AICA(1)\cdots CH_3NH_3^+}$. Thus, the geometric changes are accompanied by a notable lowering in the energy barriers of 12.8 kcal/mol ($\mathbf{TS_C\text{-}H^+}$) and 6.7 kcal/mol ($\mathbf{TS_C\cdots CH_3NH_3^+}$) with respect to $\mathbf{TS_C}$.

Location of the $\mathbf{TS_C\text{-}amide\text{-}H^+}$ and $\mathbf{TS_C\text{-}amide\cdots CH_3NH_3^+}$ transition states for the amide-assisted mechanisms confirms that they can be also facilitated by the nearby presence of a positive charge (Figures 5C and 6C). The structural changes observed in these TSs with respect to the $\mathbf{TS_C\text{-}amide}$ are particularly important for the $\mathbf{TS_C\text{-}amide\text{-}H^+}$ and are more attenuated in the $CH_3NH_3^+$-interacting structure. For example, the N−H bond developing to the departing ammonia is shortened by 0.211 and 0.093 Å at $\mathbf{TS_C\text{-}amide\text{-}H^+}$ and $\mathbf{TS_C\text{-}amide\cdots CH_3NH_3^+}$,respectively, whereas the nucleophilic attack by the 5-amino group in these TSs is clearly shifted to an earlier stage, in which the forming C−N bond is elongated by 0.831 and 0.389 Å (Figures 4C, 5C, and 6C). The presence of $CH_3NH_3^+$ reduces by 7.1 kcal/mol the energy barrier of the amide-assisted mechanism, whereas the effect of N3-protonation lowers this barrier by 12.5 kcal/mol consistent with its greater structural and electronic consequences. Interestingly, these energetic changes due to N3-protonation or $CH_3NH_3^+$-interaction parallel those observed in the uncatalyzed process, comparing the $\mathbf{TS_C}$, $\mathbf{TS_C\text{-}H^+}$, and $\mathbf{TS_C\text{-}CH_3NH_3^+}$ states. When the catalytic effects of the 4-carboxamide group are combined with the increased acidity of the 5-amino substituent through N3-protonation or strong interaction with the methylammonium moiety, the proton transfer from AICA to the formamide N atom is greatly favored, and the computed B3LYP/6-31G* barriers have values of 20−25 kcal/mol.

Thermodynamics of the Reaction. In accord with the isodesmic character of the aminolysis reaction of formamide, the gas-phase free energy of reaction ($\Delta G_{gas-phase}$) corresponding to separate products (i.e., ammonia + 4-formylamino-5-carboxamide imidazole) is slightly exothermic (−3.0 kcal/mol). Solvent effects would disfavor this process thermodynamically, given that inclusion of the PCM solvation energies predicts a free energy of reactions in aqueous solution of +6.3 kcal/mol. Overall, these values for the reaction energy are in acceptable agreement with the value of the equilibrium constant experimentally observed for the acylation of AICAR ($K_{eq} \approx 0.02$).[4]

Effect of Thiocarboxamide Substitution. It has been shown experimentally that the replacement of the 4-carboxamide group of AICAR by thiocarboxamide leads to a substrate analogue which shows a 60-fold reduction in the rate of formyl transfer catalyzed by the AICAR Tfase enzyme.[4] Thus, the theoretical examination of the aminolysis reaction between a thio-AICA model compound could be of interest to better understand the

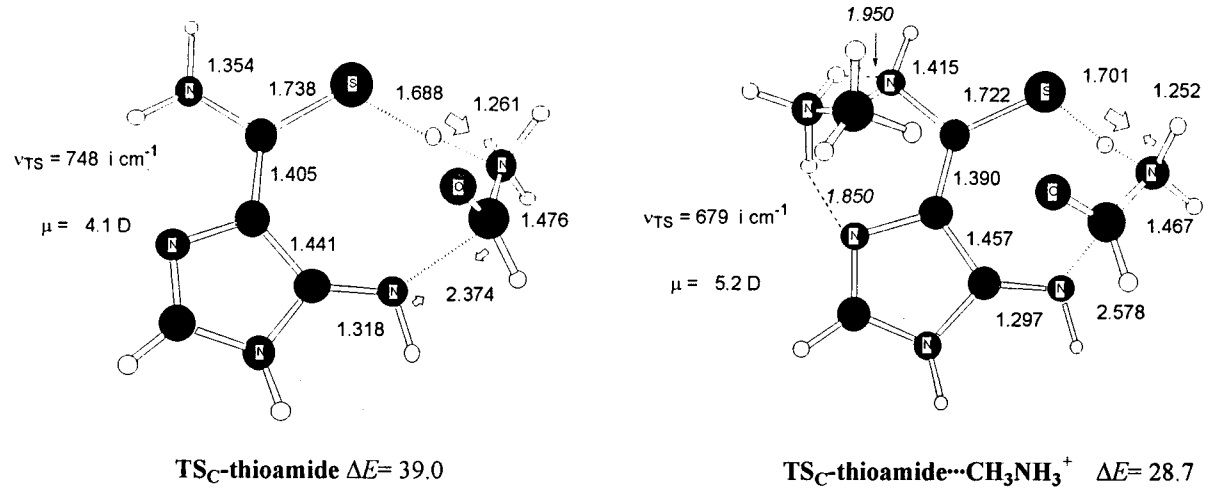

Figure 7. Optimized structures of the TSs for the aminolysis reaction between formamide and the thiocarboxamide-substituted AICA models. Distances in Å. NPA charges with hydrogens summed into heavy atoms in boldface characters. B3LYP/6-31G* relative energies including the ZPVE correction (Δ*E* in kcal/mol) are also shown.

experimental results. The thioamide-assisted pathway was characterized for the neutral form of thio-AICA and its CH_3-NH_3^+-interacting form (a TS for a N3-protonated form could not be located due to the extremely flat character of the electronic B3LYP/6-31G* PES). These pathways are analogous to those previously described for the reaction between AICA and formamide. Figure 7 displays the corresponding thioamide-substituted TSs and their relative energies.

The calculated energy barrier for the thioamide-assisted mechanism of the neutral AICA-thio compound amounts to 39.0 kcal/mol, 6.8 kcal/mol above that for the amide-assisted process. This energy difference is well understood in terms of the hydrogen-bonding ability of the thiocarboxamide which is weaker than that of carboxamide (e.g., we found that a thio-AICA isomer having the S atom protonated does not exist as a critical point on the electronic B3LYP/6-31G* PES). When CH_3-NH_3^+ interacts with the imidazole ring and the thiocarboxamide group, the energy barrier of the thioamide-assisted mechanism (28.7 kcal/mol) is stabilized by 10.3 kcal/mol. With respect to the amide-assisted process, thioamide substitution increases the energy barrier by 3.6 kcal/mol in the $CH_3NH_3^+$-interacting energy profile. We note that the sign and magnitude of this energy difference are in agreement with experimental data.

Discussion

Previous studies on substrate analogues indicated that the 4-carboxamide of AICAR is critical in formyl transfer. We proposed that it traps the putative addition intermediate by removing the proton of the 5-amino group of AICAR and mediates proton transfer to the nitrogen of the leaving group in a proton-shuttling mechanism. This mechanism is consistent with the 60-fold reduction in the rate constant we have assigned to the chemical step of transfer when the carboxamide is substituted with thiocarboxamide which is a weaker hydrogen-bonding base.[4] In a further effort to gain support for the mechanism and to elucidate roles for the active-site residues, we carried out experiments involving pH-dependent kinetic analysis of wild type and mutant enzymes bolstered by quantum chemical calculations.

The pre-steady-state burst kinetics suggested that the k_{burst} values represent the chemistry step in the pH range investigated as they were 8−10 times higher than the steady-state rate and were not affected by changes in substrate concentrations. The k_{burst} values are nearly invariant over the pH range, 6−10.5 (Figure 1), and do not implicate an ionizable group in this step over the pH range used. This observation is consistent with the amide-assisted mechanism. However, it is still possible that a catalytic group whose pK_a is beyond the pH range is involved in catalysis. A recently partially refined X-ray crystal structure of the bifunctional enzyme complexed with AICAR revealed that His267 and Lys266 are located in the AICAR Tfase active site in proximity to the imidazole moiety, but at this level of resolution no definitive statement can be made about the nature of their interactions.[6] These two residues are highly conserved across species, such as human, avian, *E. coli*, *Salmonella typhimurium*, and *Bacillus subtilus*. Mutant proteins, H267A, H267Q, K266A, or K266Q, appear to show no detectable AICAR Tfase activity while their IMP CHase activity is intact. Each mutant retained binding affinity to AICAR.[18] We also confirmed that the H267A enzyme showed no detectable AICAR Tfase activity over a broad pH range while retaining ability to bind AICAR. This result suggests that both His267 and Lys266 play critical roles in catalysis. Unfortunately, due to the lack of any detectable activity from these mutant enzymes, we were unable to conduct pH-dependent kinetics to investigate their roles in catalysis.

To investigate the feasibility of the amide-assisted mechanism, quantum chemical calculations were performed on a model system, a reaction between AICA and formamide. The results supported our hypothesis and provided additional insights into the mechanism. First, the 4-carboxamide group clearly provides a catalytic effect (8.1 kcal/mol) [**TS$_C$** (Figure 4B) and **TS$_C$-amide** (Figure 4C)]. This energy difference corresponds to a rate increase[19] of 7.4×10^5. Second, formation of the protonated carboxamide intermediate [**AICA(2)**] is highly unlikely, and it would appear only transiently as it is less stable than the transition-state structure (**TS$_H$**) for proton transfer from the 5-amino group (Figure 4A). Third, the reaction mechanism is concerted such that proton transfer from the 5-amino to the 4-carboxamide and subsequently to formamide occurs simultaneously with nucleophilic attack.

Protonation on the N3 of the AICA imidazole has a considerable kinetic effect on the aminolysis reaction of AICA by facilitating the intermolecular proton transfer from the

(18) Beardsley, G. P. Personal Communication.
(19) Calculated with $\Delta E_1^{\ddagger} - \Delta E_2^{\ddagger} \approx \ln(k_2/k_1) \times 0.592$ (kcal/mol).

5-amino group to the departing ammonia. This effect can be well understood in terms of the reinforced electron-withdrawing ability of the imidazole ring which in turn stabilizes the imino form of the 5-amino group without affecting the recipient of the proton (formamide). In fact, the calculations confirmed this reasoning given that the energy barriers for formyl transfer were significantly lowered when the imidazole of AICA was protonated by 12.8 and 12.5 kcal/mol for the uncatalyzed (Figure 5B) and amide-assisted process (Figure 5C), relative to the corresponding process in the unprotonated AICA model system (Figure 4B,C). Because such a decrease in an energy barrier corresponds to a dramatic increase in rate as expected in enzymic catalysis, protonation of the imidazole of AICAR might be a major driving force in catalysis of AICAR reaction. Still, as in the unprotonated AICA model system, proton transfer from the 5-amino to 4-carboxamide does not lead to a stable structure [**AICA(2)-H**$^+$] (Figure 5A), and argues for a concerted process.

To find out whether the protonation of AICAR is physiologically relevant, we determined by NMR the pK_a value of the imidazole of AICAR to be 3.23 ± 0.01, rather lower than the usual p$K_a \approx 6$ for imidazole. This reduced pK_a value could be due to an interaction with the phosphate group of AICAR. However, the pK_a value of the imidazole of formyl-AICA (without the phosphate group) was also found to be 2.53 as measured by UV spectroscopy.[20] In addition, the intrinsic basicity of a series of 4-substituted AICA compounds, as measured by their proton affinities (PA) in the gas phase, is substantially lowered with respect to the unsubstituted case owing to the inductive effects of these groups stabilizing the neutral form of AICA (Table 2). We also note in Table 2 that these changes in the PA values can result in a lowering of the base strength by several pK_a units with respect to the 4-unsubstituted structure. Thus, AICAR appears to have the neutral form of the imidazole under physiological conditions, implying that AICAR binds to the active site in this form. This is consistent with the lack of pH dependence found in the chemistry step from pH 6−10.5, inferring that the protonation of the AICAR imidazole probably does not occur through perturbation of its pK_a within the enzyme's active site.

However, a situation similar to protonation of the imidazole could be accomplished by an interaction of the imidazole with a general acid in the active site. One very likely candidate for this functionality is Lys266 in the active site as it would probably exist in a protonated form under physiological conditions. Quantum chemical calculations were performed on a model system with AICA complexed with $CH_3NH_3^+$ that mimics the Lys residue. Assuming that the N3 atom of AICAR establishes a short N3···H−N hydrogen-bonding interaction with the ammonium group, the charge density of the imidazole ring would be polarized in a manner similar to that found in the N3-protonated system. In addition, the ammonium group could bridge to the carboxamide N atom via a second N···H−N contact. These strong N−H···N contacts between AICA and the ammonium group (∼30 kcal/mol of binding energy) could provide one of the major binding determinants for the proper preorganization of the AICAR substrate. On the other hand, the N−H···N contacts make the imidazole ring a more electron-withdrawing group, increasing the rate of the aminolysis reaction, owing to a more favorable proton-shuttling pathway that more than compensates for the reduction in the nucleophilicity of the 5-amino group.

Again, energy barriers for both the uncatalyzed and the amide-assisted mechanism were lowered from those of the unprotonated AICA model system although the energy gain (∼7 kcal/mol) is less than that of the AICA-H$^+$ model system (Figure 6B,C). The relative stability of **TS$_C$-amide···CH$_3$NH$_3^+$** confirms again that the catalytic impact of the 4-carboxamide substituent can diminish the activation energy barrier by facilitating the intramolecular proton-transfer process in a concerted process.

To identify Lys as a general acid catalyst, we prepared the K266R mutant, since Arg should have a positively charged guanidine function under physiological conditions. The K266R mutant indeed showed AICAR Tfase activity with a 150-fold reduction in k_{cat} and little change in K_m values from those of the wild type (Table 1). However, it did not show a burst in the pH range 6−10.5 (Figure 2), indicating that k_{cat} probably measures the rate of the chemical step. The k_{cat} values exhibited no pH dependence at low pH, but increased slightly after pH 9. The limiting slope on the basic limb was much less than 1, and did not implicate an active-site ionizable group as responsible for this deviation. It could not be ascribed to a change in the structure of the reactants and products at different pH because $\Delta\epsilon_{298}$ for the reaction remained constant, nor was background amide hydrolysis detected over the pH range used. This deviation was not seen in the k_{burst}-pH profile for the wild-type enzyme, suggesting that this behavior may be ascribed to a change in the active-site environment at higher pH when Lys was replaced with longer-chain Arg.

The fact that only an Arg mutation for the Lys266 produced an active enzyme is in line with the prediction of the quantum chemical calculations that Lys might act as a general acid catalyst. It also explains the lack of pH dependence on the chemistry step as the pK_a value of Lys266 should lie outside of the pH range used. However, His267 might also play a critical role in catalysis as no activity was detected in any of the mutants derived by amino acid substitution for His267. Yet, His267 is not implicated in acid−base catalysis in the pH range used. Most likely, His267 may have a hydrogen-bonding interaction with Lys266, positioning Lys266 to have a hydrogen bond with the imidazole N3 of AICAR in the enzyme active site. In such a case, we might not observe its pK_a in the pH range used, owing to a shift in the pK_a of His267 to less than 6. A similar arrangement has been detected in the mechanism of GAR Tfase, where Asp144 forms a salt bridge to His108 and positions it to act as a general acid catalyst.[2]

Therefore, the amide-assisted pathway in the presence of $CH_3NH_3^+$ constitutes an attractive model system to explain the AICAR Tfase mechanism. In this model, the energy barrier has a moderate value (∼25 kcal/mol), and the positive charge is placed on a basic group with typically a high pK_a value. Most importantly, the $CH_3NH_3^+$-interacting AICA model nicely explains the fact that mutation of the positively charged Lys266 residue reduces dramatically the rate of the formyl transfer reaction in the AICAR Tfase active site. Moreover, this model stresses the importance of the 4-carboxamide of AICAR in binding and catalysis in agreement with all of the evidence obtained from 4-substitued analogues of AICAR.[4] Finally, the experimentally observed increment in the energy barrier as a consequence of 4-thiocarboxamide substitution is also reproduced, the calculated energy barrier of the corresponding 4-thiocarboxamide-substituted model being 3−4 kcal/mol above that of the AICA···$CH_3NH_3^+$.

Collectively, these experimental and theoretical analyses lead us to propose a mechanism for AICAR Tfase catalysis shown in Figure 8. In this mechanism, Lys266, with the aid of His267, acts as a general acid catalyst to interact with the N3 of the

(20) Baggott, J. E.; Krumdieck, C. L. *Biochemistry* **1979**, *18*, 3501−3506.

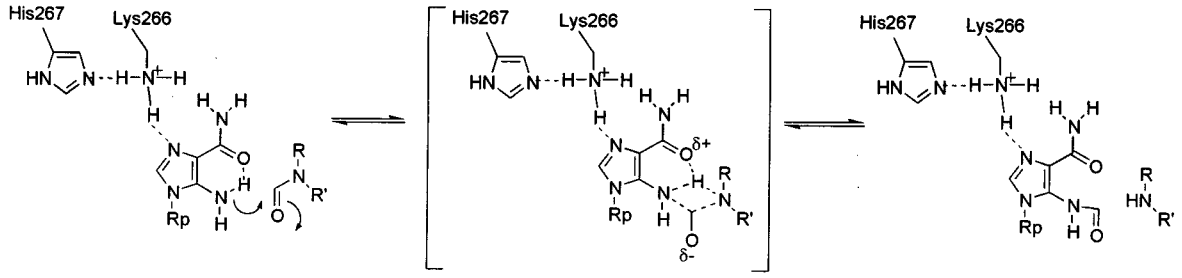

Figure 8. Proposed mechanism of AICAR Tfase. Lys266 acts as a general acid catalyst to interact with the N3 of the imidazole ring of AICAR. His267 aids Lys266 to be in the right position for a hydrogen-bonding interaction. The 4-carboxamide mediates proton shuttling from the 5-amino to the 4-carboxamide facilitated by the intramolecular hydrogen bond, and then to the nitrogen of the leaving group with simultaneous nucleophilic attack of the 5-amino group to the formyl group of folate. The protonated 4-carboxamide species is only present transiently.

imidazole ring of AICAR. The 4-carboxamide mediates proton shuttling from the 5-amino to 4-carboxamide and then to the nitrogen of the leaving group with simultaneous nucleophilic attack of the 5-amino group on the formyl group of folate. The first proton transfer is facilitated by the intramolecular hydrogen bond in the ground-state AICAR. The theoretical results suggest that protonation of the nitrogen of the leaving group is the critical event in the aminolysis reaction between AICAR and formyl group rather than the nucleophilic attack on the carbonyl group. The central role assigned to proton transfer compensates for the low nucleophilicity of the AICAR 5-amino group. High-resolution crystal structures of ternary complexes coupled with incisive kinetic studies of appropriately mutated enzymes should further test our mechanistic hypothesis.

Acknowledgment. This work was supported by the National Foundation for Cancer Research and PHS Grant GM24129 from the National Institute of Health (S.J.B.) and GM44974 from the National Institute of Health (K.M.M.).

JA010014K